600A99056

Fine Particle Emissions from Residual Fuel Oil Combustion: Characterization and Mechanisms of Formation

William P. Linak*, C. Andrew Miller
Air Pollution Prevention and Control Division, MD-65
National Risk Management Research Laboratory
U.S. Environmental Protection Agency
Research Triangle Park, NC 27711 USA

Jost O.L. Wendt
Department of Chemical and Environmental Engineering
University of Arizona
Tucson, AZ 85721 USA

Prepared for presentation at
5th International Conference on
Technologies and Combustion for a Clean Environment
July 12-15, 1999
Lisbon, Portugal

*corresponding author
tel: (919) 541-5792
fax: (919) 541-0554
e-mail: linak.bill@epa.gov

ABSTRACT

The characteristics of particulate matter (PM) emitted from residual fuel oil combustion in two different types of combustion equipment were compared. A small commercial 732 kW rated fire-tube boiler yielded a weakly bimodal particulate size distribution (PSD) with over 99% of the mass contained in a broad coarse mode, and only a small fraction of the mass in an accumulation mode consistent with ash vaporization. Bulk samples collected and classified by a cyclone indicate that 30 to 40% of the total particulate emissions were less than approximately 2.5 μm aerodynamic diameter ($PM_{2.5}$). The coarse mode PM was rich in char, indicating relatively poor carbon burnout, although calculated combustion efficiencies exceeded 99%. This characteristic behavior is typical of this type of small boiler. Larger scale utility units firing residual oil were simulated using an 82 kW laboratory refractory-lined furnace. PM emissions from this unit were in good agreement with published data including published emission factors. These data indicated that the refractory-lined combustor produced lower total but greater fine particulate emissions, as evident from a single unimodal PSD centered approximately around 0.1 μm diameter. Bulk cyclone segregated samples indicated that all the PM were smaller than $PM_{2.5}$, and loss on ignition (LOI) measurements suggested almost complete char burnout. These results have particular significance in considering the effects of fuel oil combustion equipment type on the characteristic attributes of the fine PM emitted into the atmosphere, and their ensuing health effects.

In both experiments, PSDs were determined by electrical mobility for the submicron range and by laser light scattering for the larger particles, with a small region of overlap. The PSDs, size segregated particle analyses, and observed particle morphology of both samples provided insight into mechanisms governing the formation of fine particles during residual oil combustion. Metals do not vaporize until the char burnout regime of residual oil combustion. Once liberated, these trace elements form new particles via homogeneous nucleation followed by particle growth by way of coagulation and heterogeneous condensation processes. Differences in the PSDs are explained by differences in the heat extraction rates and resulting flame quenching typical of the two combustion systems. The large coarse mode and high LOI values determined for the small fire-tube boiler suggest incomplete char oxidation due to flame quenching and only partial vaporization of the inherent trace elements. The large accumulation mode and nearly zero LOI values for the refractory-lined combustor suggest almost complete char oxidation and vaporization of the inherent trace element species. These conclusions are supported by thermodynamic and aerosol growth models.

INTRODUCTION

This paper comprises the first of a two-part communication describing results of collaborative research between combustion engineers and inhalation toxicologists. The objective is to try to establish links between the characteristics of size segregated speciation of fine particulate matter (PM) in combustion exhausts and mechanisms through which fine PM causes respiratory distress. The work reported here is concerned with the engineering portion of the work, and focuses on both characterization and mechanisms of formation of ash aerosol emissions from the combustion of residual fuel oil.

In a previous study, Miller et al. (1998) explored the relationship between residual fuel type and composition and the physical and chemical characteristics of PM produced. Four different residual fuel oils, including two grades and three sulfur contents, were burned in the same in-house 732 kW (2.5×10^6 Btu/hr) rated fire-tube boiler. In addition to tests examining four different residual fuel oils, one oil was burned under conditions designed to simulate off-optimum boiler operation. In contrast to this previous work, the current paper explores, for a single residual fuel oil, the mechanistic relationships between combustion configuration and the physical and chemical characteristics of PM produced. Whereas the previously reported work examined the effects of fuel oil compositions, this paper describes the effects of different combustion equipment types. The results of both studies are used as the basis for ultimately linking measures of acute pulmonary damage to engineering variables.

Fine particles in the air have been of considerable environmental interest in recent years because of a number of research studies correlating short term exposure of ambient levels of fine PM with acute adverse health effects (Wilson and Spengler, 1996). These studies were summarized by the EPA (U.S. EPA, 1996a; Bachmann et al., 1996) and reviewed by EPA's Clean Air Scientific Advisory Committee (CASAC) which concluded there was evidence linking ambient fine PM concentrations and adverse health effects (Wolff, 1996). These studies were the basis for a revision of the National Ambient Air

Quality Standards (NAAQS) for PM that included a standard for PM less than 2.5 μm in diameter ($PM_{2.5}$) (Federal Register, 1997).

In the ambient atmosphere, ultrafine PM, which includes a portion of $PM_{2.5}$, is composed primarily of sulfates, nitrates, condensed organics, carbonaceous soot, and inorganic aerosols formed during high temperature processes such as the combustion of fuels containing trace quantities of metals and other impurities (U.S EPA, 1996a; Linak and Wendt, 1993, 1994). Formation of these small particles is heavily influenced by condensation and other gas-to-particle conversion processes. In contrast, the coarse fraction of PM tends to be composed of particles formed by mechanical (e.g., fragmentation, grinding, crushing, and entrainment) processes. Because they are formed by different mechanisms, the fine and coarse fractions of PM are likely to have significantly different compositions. Particle composition has been identified as one of the possible factors driving the adverse health effects associated with exposure to ambient PM (National Research Council, 1998).

Health effect researchers have identified at least two aspects of particle composition that appear to exacerbate health damage from particles. The first is related to water-soluble transition metals such as copper (Cu), iron (Fe), vanadium (V), nickel (Ni), and zinc (Zn) present in the particles (Dreher et al., 1996a, 1996b, 1997). The second aspect of particle composition that might be important as far as health damage is concerned is aerosol acidity in general. In addition to these composition related facets, ultrafine particles (those particles less than 0.1 μm in diameter), regardless of composition, have been identified as potential factors influencing mechanisms for these health impacts (U.S. EPA, 1996a). Particles with all of these characteristics (transition metals, acidity, and ultrafine size) are contained in the PM generated from the combustion of residual fuel oils (e.g., No. 5 and 6 fuel oils). Hence, one might hypothesize residual fuel oil combustion to be suspect, as far as emission of toxic fine particles is concerned.

Unfortunately, the hypothesis that residual oil combustion is the prime source of fine particles causing respiratory distress is not consistent with epidemiological data. Residual fuel oils are used in significant quantities in only selected regions of the country. Discounting sales of Bunker C oil, the majority of which is likely to be burned by ships well away from continental coastlines, Figure 1 shows significant residual oil usage in the Northeast and Southeast regions. There is little residual oil usage in the Midwest or along the Pacific coast. Additionally, the 13 other Great Plains and Rocky Mountain states combined (not included in Figure 1) account for less than 1% of the residual fuel oil sales in the U.S. However, adverse health effects associated with exposure to fine PM are not limited to the Northeast and Southeast regions of the U.S. (Dockery et al., 1993). This fact suggests that sources of fine PM other than (or in addition to) those related to residual fuel oil combustion must also be important.

EXPERIMENTAL

Particle characteristics and emissions are compared from two types of combustion systems. These can be considered to represent extremes of a range of the practical conditions under which fuel oil is burned. Although they may not represent specific boilers in all respects, they are investigated here with a view to determining how this range of combustion conditions influence the characteristics of fine particles, and the mechanisms which form them. The first system is a small fire-tube boiler, in which combustion occurs in tubes surrounded by water or steam. These types of small boilers have large heat transfer surfaces, small combustor volumes, relatively small gas residence times, cold walls, and high gas quenching rates, and often produce emissions with relatively high carbon contents due to unburned carbonaceous oil residues or char. The second system is a refractory-lined research combustor designed to simulate the time/temperature environments of larger utility boilers and incinerators. In large utility boilers the water to be boiled, rather than the combustion gases, is contained in tubes. These systems, including the refractory-lined combustor, operate at higher temperatures with lower gas quenching rates. As will be discussed later, particle emissions from this

system contain very little unburned carbon and more closely approximate emissions from large oil-fired utility boilers reported in the literature.

Fire-tube Boiler

Experiments were performed using EPA's North American, three-pass, fire-tube package boiler (NAPB), which is a practical, commercially available residual fuel oil combustion unit (Figure 2). The burner was a North American model 6121-2.5H6-A65, rated at 732 kW (2.5×10^6 Btu/hr) and has both a natural gas ring and an air-atomizing center nozzle capable of firing No. 2 through No. 6 fuel oils. The main fire-tube has a diameter of 46 cm (18 in), and each of the 24 second-pass tubes and 20 third-pass tubes has an inside diameter of 6.4 cm (2.5 in). The boiler has 27.9 m^2 (300 ft^2) of heat transfer surface, and can generate up to 1090 kg/hr (2400 lb/hr) of saturated steam at gauge pressures up to 103.4 kPa (15 psig). Heat is extracted from the steam through a heat exchanger and rejected to an industrial cooling water system that provides a simulated boiler load. Oil temperature can be controlled using an in-line electric heater to maintain consistent fuel viscosity. Oil and atomizing air pressures are independently controlled to ensure proper oil atomization. The NAPB is equipped with several sampling ports located at the exit of the boiler (see Figure 2). Temperatures at these sampling ports ranged from 450 to 550 K (350 to 530 °F).

Refractory-lined Combustor

Experiments were also performed using the laboratory horizontal tunnel combustor also presented in Figure 2. Although this system has a maximum rating of 82 kW (280,000 Btu/hr), these experiments were conducted at 59 kW (200,000 Btu/hr). This refractory-lined research combustor was designed to simulate the time/temperature and mixing characteristics of practical gas- and oil-fired combustion systems. Fuel oil and combustion air were introduced into the burner section through an International Flame Research Foundation (IFRF) moveable-block variable-air swirl burner. This burner incorporates a pressure atomizing oil nozzle positioned along its center axis.

Swirling air passes through the annulus around the fuel injector, promoting flame stability and attachment to the refractory quarl. A high swirl (IFRF Type 2) flame with internal recirculation (swirl No.=1.48) was used. Gas and aerosol samples were taken from a stack location 5.9 m from the burner quarl. The temperature at this location was approximately 670 K (745 °F).

Measurements

Both the fire-tube boiler and refractory-lined combustor are fully instrumented, with continuous emission monitors (CEMs) for carbon dioxide (CO_2), carbon monoxide (CO), nitrogen oxides (NO_x), oxygen (O_2), and sulfur dioxide (SO_2). A data acquisition system was used to continuously record CEM measurements as well as boiler steam and flue gas temperatures. The flue gases from both units pass through a manifold to a facility air pollution control system (APCS). Induced drafts (necessary for the APCS operation) were imposed on both systems. All experiments were performed at a stoichiometric ratio (SR) of 1.2 (20% excess air). No air preheat was employed.

Particulate Sampling and Analysis

PM emissions were sampled using a variety of methods. Standard EPA Method 5 and Method 60 sampling and analytical procedures were used to determine total particulate and metal concentrations (Garg, 1990; EPA, 1994a, 1994b). Metal analyses were performed using acid digestion and inductively coupled plasma (ICP) mass spectrometry. Other metal analyses were determined by x-ray florescence spectroscopy (XRF). Additional samples were analyzed by x-ray adsorption fine structure (XAFS) spectroscopy. As described by Galbreath et al. (1998) and Huggins and Huffman (1999), XAFS spectroscopy is a non-destructive element-specific structural probe that is useful for determining trace element speciation and forms of occurrence in chemically and structurally complex materials like combustion ash. XAFS spectroscopy is intended to compliment other techniques (such as ICP and XRF spectroscopy) and was used here to help determine sulfur speciation within the collected PM.

PSDs were determined by three techniques: electrical mobility and inertial impaction for sampled aerosols and light scattering for in-situ in-stack analyses. Extractive samples were taken for collection by inertial impaction and electrical mobility analyses using an isokinetic aerosol sampling system based on the modified designs of Scotto et al. (1992) and Linak et al. (1994). In order to minimize in-probe gas and aerosol kinetics, the sampling system dilutes and cools the aerosol sample using filtered nitrogen immediately after sampling. Dilution ratios, here approximately 5:1, are determined for each experiment and can be verified independently by the measurement of a nitric oxide tracer gas. Diluted samples were directed to a Thermo-Systems Inc. scanning mobility particle sizer (SMPS). The SMPS classifies and counts particles within a working range of 0.01 to 1.0 μm diameter using principles of charged particle mobility through an electric field. The SMPS was configured to yield 54 channels evenly spaced (logarithmically) over a 0.01 to 1.0 μm diameter range.

Extracted samples during the fire-tube boiler experiments were also directed to an Andersen Inc. eight-stage, 25 L/min. (0.9 ft^3/min), atmospheric pressure in-stack cascade impactor. This instrument is designed to collect samples on nine stages (including the afterfilter) less than approximately 10 μm in diameter for subsequent gravimetric and chemical analysis. The in-stack cascade impactor was operated using a modified California Air Resources Board (CARB) Method 501 procedure (CARB Method 501, 1990). Procedure modifications are discussed in detail elsewhere (Miller et al., 1998). During the refractory-lined combustor experiments, a MSP Inc. 10-stage, 30 L/min (1.06 ft^3/min) Micro-Orifice Uniform Deposit Impactor (MOUDI) was used. This atmospheric pressure impactor is designed for enhanced small particle resolution.

In addition to the electrical mobility and inertial impaction devices, which require an extracted sample, in-situ light scattering PSDs were taken using an Insitec Inc. particle counter sizer velocimeter. Although this instrument is designed to measure both particle size and velocity, the velocity feature was not used here. This instrument determines particle size by measuring the light scattering intensity of particles which pass through a sampling volume established within the combustor stack by a laser focused through a set

of quartz optical access ports. The working range of this device was approximately 0.3 to 100 μm diameter which slightly overlapped and extended the PSD data collected by the SMPS.

Samples were also collected on silver membrane filters and analyzed using a SEM equipped with an energy dispersive x-ray (EDX) spectrometer. This provided morphological information of individual particles. Particles were extracted from the stack location using the same sampling system and dilution as used by the SMPS described above. However, these particles were directed through a stainless steel filter holder containing a 47 mm silver membrane filter. Sampling times of approximately 30-60 s provided a sufficient quantity of particles for analysis. Silver filters were used to improve conductivity and minimize particle charging caused by the electron beam.

It was necessary to collect larger quantities of size segregated PM for the toxicological studies (described in a companion paper) and XAFS analyses. These were collected using the large dilution sampling system (see Figure 3), which is capable of sampling 0.28 m^3/min (10 ft^3/min) of flue gas. Isokinetic sampling conditions were not possible for these large dilution samples. The sample passes through a modified Source Assessment Sampling System (SASS) cyclone and is then diluted with clean ambient air [2.8 m^3/min (100 ft^3/min)] by means of a perforated cone assembly. Rapid uniform dilution within an approximate 3 s residence time mixing chamber cools the sampled gases and PM to approximately ambient temperature. The resulting PM is collected on large (64.8 cm, 25.5 in) Teflon coated glass fiber filters, transferred to sampling jars, and made available for subsequent chemical, physical, or biological analysis. This sampling system was originally designed and constructed to sample particulate and condensable emissions from municipal and hazardous waste incineration facilities. Further details regarding the dilution sampler's construction and operation are presented by Steele et al. (1988). The SASS cyclone preseparator produces 50 and 95% particle collection efficiencies at approximately 1.8 and 2.5 μm aerodynamic diameter, respectively, at standard conditions.

Experimental Approach and Conditions

The current study investigated the effects of combustion configuration by comparing the characteristics of the fire-tube boiler PM reported previously (Miller et al., 1998), with the PM characteristics of the same fuel burned in the refractory-lined combustor. The high sulfur No. 6 oil used in both cases contained 2.33% sulfur. Operational characteristics for both systems included similar oil temperatures (380 to 400 K, 230 to 250 °F) and stoichiometries (SR=1.2), corresponding to stack O_2 concentrations of approximately 3.5% (dry).

Figure 4 presents an oil droplet PSD for the high sulfur No. 6 fuel oil using the Delavan Airo Combustion air atomizing type oil nozzle (model 30615-84) from the fire-tube boiler. Fuel oil and atomizing air were maintained at approximately equal pressures between 200 and 240 kPa (29 and 35 psig) during boiler operation. Figure 4 indicates that this atomizer produces oil droplets with a relatively narrow PSD and a mean diameter of between 30 and 40 μm.

The refractory-lined combustor experiments used a similar air atomizing oil nozzle manufactured by Spraying Systems Co. (model Air Atom 1/4-JSS). However, in order to be incorporated within the smaller IFRF burner, a stock atomizer required extensive external modifications. Critical internal dimensions were unaffected. Although no oil droplet PSD is available for the refractory-lined combustor experiments, the PSDs are believed to be similar to those for the boiler studies, and differences in carbon burnout may be attributed to differences in temperature history rather than in droplet size.

RESULTS AND DISCUSSION

Equilibrium Predictions

Multicomponent equilibrium calculations can provide insight into which species are thermodynamically stable at flame and flue gas temperatures. Previous literature on equilibrium predictions exist in the work of Wu and Biswas (1993), Frandsen et al. (1994), and Owens et al. (1995), although there are relatively few results with the inorganic ash concentration levels pertinent to residual oil combustion. As always, the accuracy of equilibrium results depends on the accuracy of the thermodynamic data available, and on the availability and inclusion of thermodynamic data for all important species containing the elements in question. In addition, concentration predictions based on equilibrium calculations may not be realized in practical systems, because they do not take into account kinetic or mixing limitations. Thermochemical predictions were determined using the CEA computer code for calculating complex chemical equilibrium compositions (McBride et al., 1993). Table 1 lists the metal species considered in these calculations, together with the appropriate references. Of interest is the thermodynamic partitioning between vapor and condensed phases, as well as the partitioning between various species. Input conditions, summarized in Table 2, represent combustion of the high sulfur No. 6 oil at a stoichiometric ratio of 1.2. The fuel ultimate analysis and trace element concentrations were taken from previously published results (Miller et al., 1998). However, only trace elements with concentrations greater than 1 μg/g of oil were considered in the calculations.

Figure 5 presents the results of these equilibrium calculations for seven trace elements [V, Ni, Zn, Fe, Cu, lead (Pb), and chromium (Cr)]. Mass fractions of the elements (as indicated species) are plotted against temperature. Based on the species and thermodynamic data listed in Table 1, the elemental dew points are calculated to be approximately 1800 K for V, 1700 K for Ni, 1200 K for Zn, 1700 K for Fe, 1400 K for Cu, 1100 K for Pb, and 900 K for Cr. These predictions indicate that, at the concentrations present in fuel oil, all seven elements might vaporize within the combustion environment, depending on the local temperatures to which the ash constituents are exposed. The dewpoints are lower than those calculated for pulverized coal and incineration applications, because of the low ash and metal concentrations (Linak and Wendt, 1994), and appear to indicate possible vaporization of Cr, for

example, which is usually considered to be nonvolatile. In fact, Figure 5 indicates that $Cr_2O_3(s)$ is not a predicted condensed species at intermediate temperatures. This is in contrast to similar calculations performed using higher Cr concentrations simulating an incineration environment (Linak et al., 1996). These previous calculations examined a system containing 100 ppm_v Cr compared to the current system which contains approximately 0.03 ppm_v. It should be emphasized that only the species in Table 1 are considered in these calculations, and the presence of even small quantities of other elements may affect the predicted behavior. For example, even small amounts of chlorine can affect metal speciation and volatility (Linak and Wendt; 1993, 1994). Also evident from Figure 5 is that all seven elements are predicted to form sulfates at lower temperatures (approximately 700 to 1100 K, 800 to 1520 °F). This preferred speciation is likely to affect the solubility and perhaps the bio-availability and toxicity associated with the trace elements. However, it is possible that kinetic limitations at these low temperatures could limit the formation of thermodynamically stable metal-sulfate species.

Particle Size Distributions

The upper panel of Figure 6 presents representative particle volume distributions for the fire-tube boiler (open symbols) and refractory-lined combustor (shaded symbols) experiments. The inset in the upper panel shows more detail in the ultrafine particle size range. Together, these electrical mobility and light scattering measurements span 4 decades of particle diameters (0.01-100 μm). The fire-tube boiler PSD is the same data as plotted in Figure 3 of Miller et al. (1998). The boiler PSD indicates that most of the particle volume is associated with large (coarse mode) particles greater than 10 μm in diameter. The open symbols in the inset show that even the fire-tube boiler produces a small accumulation mode with a mean diameter of between 0.07 and 0.08 μm, but that this accumulation mode is much smaller than that for the refractory-lined furnace (shaded symbols). Thus, both configurations produced an ultrafine mode, but only the fire-tube boiler produced a bimodal PSD with a very large and dominant coarse mode.

As discussed by Miller et al. (1998), this type of bimodal PSD is consistent with a mechanism of metal vaporization/nucleation/coagulation/condensation and incomplete burnout of residual fuel cenospheres. In order to understand how these two modes arise, it is necessary to review the various important controlling mechanisms. Williams (1976) describes the sequence of events associated with residual oil combustion. Initially, fuel oil is atomized and sprayed though the burner with combustion air to produce an initial droplet size distribution ranging from less than 10 to approximately 100 μm in diameter (see Figure 4). As these fuel droplets are heated, the lighter organic components vaporize, diffuse into the gas phase, and react (self-ignite) with the oxygen forming diffusion flames around each droplet. As the process proceeds, fractional distillation, liquid-phase cracking, and thermal decomposition add vapor-phase fuel species to the flame front, causing considerable swelling of the remaining heavy tar droplet. As the volatile components are depleted, the remaining heavy tars collapse to form a carbonaceous residue (or char) with an open cell structure called a cenosphere. The flame front recedes into the cenosphere resulting in heterogeneous combustion of the carbonaceous residue at a rate of about 10% that of the initial droplet. These porous particles, composed primarily of carbon and ash, may be quite large (comparable to or even larger than the original fuel droplet) and have relatively low density. As oxygen diffuses into the cenospheres, heterogeneous combustion results in high internal temperatures promoting vaporization of the inherent mineral matter, essentially all of which is bound directly to the organic matrix. As char combustion concludes, these cenospheres produce the large supermicron (coarse mode) PSD.

Figure 7 presents a scanning electron microscope (SEM) image of oil char collected from the fire-tube boiler, and the sponge-like morphology that is apparent clearly suggests swelling and pore formation. The size of this coarse mode will be strongly dependent on the combustion environment and particularly dependent on processes that influence flame quenching. Likewise, the extent of ash (metal) vaporization is also strongly dependent on the extent of carbon burnout. When combustion is incomplete, a large portion of the metals remain trapped in the unburned char particles, and never escape into the vapor phase. However, as the combustion gases

cool, those metals which have vaporized will condense on existing surfaces or, if supersaturation partial pressures are large enough, will nucleate to form new particles. Condensation on existing submicron particles is preferred because these particles typically dominate the available surface area. The distinctive submicron peak (between 0.07 and 0.08 μm diameter) is indicative of particles formed by nucleation, coagulation, and condensation of materials that have vaporized in the high temperature region of the combustor. However, when large portions of the metal constituents fail to vaporize, as in the fire-tube boiler, the accumulation mode will be very much smaller than when they do vaporize, as in the refractory-lined combustor (see Figure 6).

In stark contrast to the fire-tube boiler volume PSD, Figure 6 indicates that the refractory-lined combustor volume PSD (shaded symbols) is composed exclusively of a narrow submicron accumulation mode with a mean diameter of approximately 0.1 μm. The light scattering measurements indicated an almost complete absence of particles greater than 1 μm diameter. This is consistent with the lack of any dilution sampler cyclone catch, the negligible LOI values, and the greenish-yellow color of the filter PM. The volume PSD for the refractory-lined combustor is the result of nearly complete char burnout and nearly complete vaporization of the trace elements. These species have undergone nucleation, condensation, coagulation, and agglomeration processes to produce the distinctive accumulation mode shown in Figure 6. Comparison between the areas under the submicron volume PSDs for the two types of equipment suggests that only a very small fraction (< 1%) of the ash is vaporized in the fire-tube boiler. In contrast, well over 99% of the ash vaporizes in the refractory lined furnace.

Comparison of Calculated and Measured Mass Concentrations

Table 3 presents a comparison of calculated and measured mass concentrations for the two experimental systems. It should be noted that these masses include both ash and unburned carbon, when present. The first two columns present typical total volume concentrations for the boiler and combustor experiments as determined by the electrical mobility and light scattering measurements, and are obtained by integration of the PSD

data presented on the upper panel of Figure 6. Total volumes are determined by the sum of accumulation and coarse mode values. Mass concentrations, calculated from these measured volume concentrations, and those measured by EPA Method 5, are presented in the next two sets of columns. A density of 3.5 g/cm^3 was assumed for the accumulation mode PM characterized by the electrical mobility measurements, and a density of 1.85 g/cm^3 was assumed for the coarse mode PM characterized by the light scattering measurements. Note that the material densities used here are not the same as ash bulk densities. These assumed densities, yielded 180 mg/m^3 for calculated mass concentrations for the boiler and 93 mg/m^3 for the combustor. Mass concentrations of 184 and 93 mg/m^3 were independently measured for the boiler and combustor experiments, respectively. The assumed density of 3.5 g/cm^3 for the accumulation mode PM was chosen as a reasonable value based on the hypothesis that these particles are composed of condensed trace element vapor (sulfates and oxides). If one estimates that the light scattering measurements did not include approximately 25% of the coarse mode volume corresponding to PM larger than 100 μm diameter (see Figure 6), then the assumed density would need be revised to approximately 1.4 g/cm^3 (instead of 1.85 g/cm^3) to reconcile the calculated and measured mass concentrations. Both values are reasonable based on densities reported for activated carbons and coal chars and based on the extensive porous particle morphology evident from Figure 7.

Emission Factors

Note that the measured mass concentration of 93 mg/m^3 determined from the refractory-lined combustor experiments can be converted into an emissions factor of approximately 10.5 lb/10^3 gal (1.26 g/L). This value is comparable to the emission factor of 9.2 lb/10^3 gal (1.10 g/L) for No. 6 residual oil-fired boilers larger than 100x10^6 Btu/hr (29.3 MW) published in AP-42 (U.S. EPA, 1996b). This comparison lends further support to the supposition that the refractory-lined combustor adequately simulates the combustion environment of larger industrial and utility boilers. Note that Table 3, Figure 6, and the lack of any dilution sampler cyclone catch indicate that the PM emissions from this unit are essentially all less than 2.5 μm aerodynamic diameter. As reported by Miller

et al. (1998), the range of emission factors determined for the fire-tube boiler was approximately twice that of oil fired utility boilers. However, dilution samples for these experiments indicate that only 30 to 50% of the PM mass emissions had an aerodynamic diameter less than 2.5 μm. Hence, the fine PM emission factor for utility boilers may well be greater than that of fire-tube boilers.

Emissions results from this study can be compared to values from the literature. Goldstein and Siegmund (1976, 1977) examined the effect of fuel type and combustion modifications on PM emissions from a small 37 kW (50 hp) fire-tube boiler. They report similar PM emissions of approximately 180 mg/m^3 with carbon contents of up to 80% while burning a similar 2.2% sulfur No. 6 fuel oil. They also noted that efforts to increase PM burnout shift the PSD toward the submicron range. Conversely, Cheng et al. (1976) and Bacci et al. (1983) examined PM emissions from 30 MW (1x10^8 Btu/hr) and 320 MW (1x10^9 Btu/hr) fuel oil fired power plants, respectively. PM emissions from these units were reported to be 87 mg/m^3 and 40 to 50 mg/m^3, respectively, even though the 30 MW unit was equipped with a multicyclone PM control system. Bacci et al. also recount particle densities ranging from 1.4 to 1.9 g/cm^3 for particles between 3 and 5 μm diameter, considerable enrichment of sulfur, V, and Ni on particles smaller than 0.5 μm diameter, and morphological and mineralogical data indicating the presence of cenospheres and micron scale crystals composed of sodium vanadium oxide hydrate. They go on to state that, even at this large scale, increased combustion chamber temperatures and improved oil atomization improve particle burnout and overall reduction of the carbonaceous PM.

Elemental Composition and Particle Size

Table 4 presents a comparison of the trace element emissions for the fire-tube boiler and refractory-lined combustor experiments. As expected, these concentrations are similar due to the fact that both systems fired the same high sulfur No. 6 fuel oil. However, in contrast to the PM from the boiler which exhibited high values for loss on ignition (LOI) ranging from 60 to 85%, blank-corrected results of filter samples from the

combustor tests indicate no mass lost on ignition. The sum of the concentrations of the seven analyzed elements listed in Table 4 for the combustor experiments account for 21.6 mg/m^3 or approximately 23% of the total mass emissions. However, if these elements are assumed to exist as sulfates, they then account for 67.1 mg/m^3 or approximately 72% of the total mass emissions. In fact, XAFS spectroscopy indicated that, while a large portion (40-60%) of the sulfur measured in the fire-tube boiler PM existed as unoxidized organic sulfur (predominantly thiophenic sulfur), essentially all (99%) of the particulate bound sulfur in the refractory-lined combustor samples was in the form of sulfates.

Figure 8 presents elemental mass fractions vs. particle diameter for six metals and sulfur from the refractory-lined combustor tests. Impactor substrates from replicate experiments were analyzed by XRF and ICP spectroscopy for the six metals. Sulfur and sulfate loadings were determined by XRF and ion chromatography (IC) analysis, respectively. Figure 8 plots elemental mass fractions normalized by dlogDp vs. the characteristic aerodynamic diameter for each impactor stage. The data indicate that, in general, XRF and ICP analyses produce similar results, and that the emissions of these elements are concentrated in particles approximately between 0.08 and 0.2 μm diameter. This corresponds to the accumulation mode determined by the electrical mobility analyzer (see Figure 6). Figure 8 also indicates that sulfur and sulfates are present within particles of the same size. It is interesting to note that Figure 8 also indicates the presence of a small but distinct mode at approximately 1 μm diameter. This small mode is noted in the replicate V, Ni, and Zn measurements determined by XRF and ICP analysis, and possibly in the Cu XRF analysis. This mode is not evident for the more volatile metal, Pb. These data are consistent with the conjecture that less volatile metals are released very late during the heterogeneous combustion of the cenospheric carbon and only as the neighboring carbon atoms are oxidized, while more volatile metals can more easily vaporize from interior surfaces and diffuse to the gas-phase environment exterior to the char particle. The 1 μm diameter particles noted in Figure 8 may be the result of nonvolatile metal coalescence as the last vestiges of carbon are consumed. Note that the corresponding volume PSD in Figure 6 does not indicate the presence of this small mode,

although this may be the result of relatively poor sensitivity of the light scattering measurements at the lower limit of its operational range.

Model Predictions

Experimental results were compared to model predictions using a multi-component aerosol simulation code (MAEROS). The purpose of these calculations was to illustrate that the resulting PSDs for both systems could be predicted using the same modeling approach involving char particle burnout (or premature quenching) followed by homogeneous nucleation and coagulation of a portion of the PM mass. A secondary objective was to determine the extent to which differences in coagulation rates caused by large differences in vaporized mass and resulting number densities might account for the differences in the measured PSDs. The MAEROS code was developed by Gelbard and Seinfeld (1980) to simulate the dynamics of a spatially homogeneous aerosol. The algorithms solve a discrete form of the general dynamic equation (GDE) which describes the spatial and temporal evolution of a particle size distribution including convective and diffusive terms. The GDE can include terms to describe: coagulation due to Brownian motion, gravity, and turbulence; particle deposition due to gravitational settling, diffusion, and thermophoresis; particle growth due to condensation of a gas; and time varying sources of particles of different sizes and chemical compositions. MAEROS is intended as a general tool to supply necessary algorithms to solve the GDE for aerosol and other particulate systems. Figure 9 illustrates the predicted evolution of an aerosol due to coagulation. The particle size domain (0.001 to 20.0 μm diameter) was divided into 13 geometrically equal sections or bins. Coagulation was the only mechanism considered. All other mechanisms (condensation, nucleation, deposition, etc.) were disabled. Two cases corresponding to the fire-tube boiler and refractory-lined combustor conditions were examined.

To examine particle evolution within the fire-tube boiler, 99.8% of the 180 mg/m^3 PM mass was assigned to the various sections so as to simulate the coarse mode mass PSD illustrated in Figure 6. The remaining 0.2% of this mass was assigned to section 2

(0.0021-0.0046 μm diameter) to simulate the nucleation of a vapor fume. This distribution between fine and coarse mode PM corresponds to the ratios determined by the electrical mobility and light scattering instruments (see Table 3). The initial number concentration was 1.5×10^{16} /m^3, and it is important to note that, while the nucleating vapor comprised only 0.2% of the PM mass, it comprised well over 99.99% of the PM number. System pressure and temperature were maintained at 1.01×10^5 Pa (1 atm) and 810 K (1000 °F) to simulate post-flame conditions. Following from this initial distribution, Figure 9 presents three mass distributions which follow the evolving aerosol through three orders in time (t=0.1, 1.0, 10 s). Note that coagulation does not change the total aerosol mass and that the areas under all three curves represent 180 mg/m^3. Number concentrations, however, are affected, At 0.1 s, the number concentration has fallen to 1.1×10^{16} /m^3, and the average nuclei size has grown slightly. At 1.0 and 10.0 s, the distributions have grown somewhat further into the 0.01 to 0.1 μm diameter range. These times represent a range of typical residence times within combustion systems. At 10 s, number concentrations have fallen to 1.2×10^{14} /m^3 and the nuclei are accumulating in a mode with a mean diameter of approximately 0.02 μm (see Figure 9 insert). The distribution of the coarse mode PM is relatively unaffected by these processes.

In contrast to the boiler simulation, 100% of the 90 mg/m^3 PM mass measured in the refractory-lined furnace was assigned to section 2. Again, this initial distribution corresponds to the partitioning seen in Table 3, and indicates complete oxidation of the oil char and vaporization of the inorganic elements followed by homogeneous nucleation of these elements to form 20 to 40 Å particles. The initial number concentration is 2.7×10^{18} /m^3. In comparison to the boiler simulation, Figure 9 indicates that these aerosol nuclei tend to coagulate much more quickly, due to the much larger number concentration of nuclei particles. At 1 and 10 s, as number concentrations fall to 8.2×10^{14} and 7.6×10^{13}, respectively, coagulation slows considerably causing the aerosol to accumulate into a mode approximately between 0.07 and 0.2 μm diameter. Coagulation processes predict that the accumulation mode produced from the refractory-lined combustor would be larger in diameter compared to the accumulation mode produced from the fire-tube boiler. This prediction is reflected in the measurements. The

accumulation mode measured from the refractory-lined combustor matches the predicted PSD (see Figure 6), while the predicted accumulation mode for the fire-tube boiler (0.02 μm diameter) slightly underpredicts the measured value (0.07 μm diameter). Heterogeneous condensation of a portion of the vapor on existing nuclei is a competing process which has been shown to increase particle growth rates (Davis et al., 1998). Note that the coagulation mechanism described in Figure 9 also does not include the effect of differing fractal properties of any agglomerates that may be formed (Matsoukas and Friedlander, 1991). It has been assumed here that only spheres result from the coagulation process.

CONCLUSIONS

The effects of combustion configuration on fine particle emissions from residual fuel oil combustion were examined. A laboratory scale refractory-lined combustor, which was shown to simulate combustion conditions of a large utility residual oil fired boiler (as far as particulate emission factors were concerned) produced fly ash particles with an essentially unimodal PSD with a mean diameter of approximately 0.1 μm. Conversely, a pilot scale fire-tube package boiler produced particles with a weak bimodal size distribution, which included a small fraction (~0.2%) of the mass with particle diameters less than 0.1 μm and a large fraction (~99.8%) of the mass with particle diameters between 0.5 and 100 μm. Here the large particles were shown to consist of large porous carbonaceous cenospheres resulting from poor carbon burnout, and this characteristic is not uncommon for that class of equipment. Although the total particulate mass concentrations in the flue gas of the refractory-lined combustor were less than half of those of the fire-tube combustor, ultrafine particle concentrations of the refractory-lined combustor were notably larger than those of the fire-tube boiler. Volume PSDs obtained from two independent particle sizing instruments were, with only a few very reasonable assumptions, consistent with independently measured total mass emission rates for both equipment types.

The results presented here provide insight into mechanisms of fine particle formation from residual oil combustion. For the refractory-lined combustor, where very few large particles were formed, the PSD was nearly unimodal with a mean diameter of approximately 0.1 μm. These particles were composed primarily of trace species containing V, Ni, Zn, Fe, Cu, and sulfur. Additionally, these particles contained very little carbon (based on LOI) and the particulate bound sulfur was speciated almost exclusively as sulfates. The fire-tube boiler produced PM with weak bimodal behavior. A portion (predominantly metals and sulfur) reporting to a small mode with a mean diameter of approximately 0.7 to 0.8 μm, and a large portion (comprised primarily of char) producing a broad coarse mode with a mean diameter of approximately 40 to 50 μm. Both of these types of behavior provide circumstantial evidence for a mechanism of fine particle formation from residual oil combustion as follows. Commonly considered nonvolatile metals are likely released into the gas phase during the last stages of carbon burnout, and this is why the accumulation mode for particles formed from vapor nucleation was so small for the fire-tube boiler. For the refractory-lined combustor, where char burnout was nearly complete, most of the nonvolatile metals were released into the gas phase, except for a small residual amount (not detected in the volume PSDs - Figure 6) that may have coalesced with other metal species at the very end of char burnout. Volatile metals, such as Pb, may vaporize earlier in the process and diffuse through the char to the gas phase. Hence, the Pb-containing particulate PSD has a strictly unimodal behavior.

Further insight was gained through mathematical modeling of the aerosol dynamics, the predictions from which were compared to experimental measurements. In each case, it was assumed that 2 to 4 nm nuclei formed from a vapor-phase metal fume, and then allowed to grow by coagulation. The fire-tube package boiler measured PSDs were consistent with a model in which 0.2% of the final particulate mass (approximately 0.4% of the fuel oil ash) was at one time nuclei (formed from vaporized trace elements), and evolved via coagulation. These nuclei do not readily interact with the coarse mode of unburned carbonaceous cenospheres due to the large differences in particle number concentrations. The refractory-lined combustor PSDs were predicted using the same

model, but with 100% of the final particulate loading being assigned to nuclei in the 2 to 4 nm range. This arrangement yielded a PSD which compared well with the measured PSD. Hence, these theoretical calculations strongly supported the mechanisms of fine particle formation described above.

ACKNOWLEDGMENTS/DISCLAIMER

Portions of this work were conducted under EPA Purchase Order 8CR244NASX with J.O.L. Wendt and EPA Contract 68-C-99-201 with ARCADIS Geraghty & Miller. The authors gratefully acknowledge the contributions of C. Elmore, C. King, E. Squier, and D. Janek of ARCADIS Geraghty & Miller to the experimental efforts, and to S. Wasson, P. Groff, and M. Calvi of EPA-APPCD and G. Huffman and F. Huggins of the University of Kentucky for analytical support. The research described in this article has been reviewed by the Air Pollution Prevention and Control Division, U.S. Environmental Protection Agency, and approved for publication. The contents of this article should not be construed to represent Agency policy nor does mention of trade names or commercial products constitute endorsement or recommendation for use.

REFERENCES

Bacci, P., Del Monte, M., Longhetto, A., Piano, A., Prodi, F., Redaelli, P., Sabbioni, C., and Ventura, A., Characterization of the particulate emission by a large oil fuel fired power plant, J. Aerosol Sci., 14(4), 557-572 (1983).

Bachmann, J.D., Damberg, R.J., Caldwell, J.C., Edwards, C., and Koman, P.D., Review of the National Ambient Air Quality Standards for Particulate Matter: Policy Assessment of Scientific and Technical Information, EPA-452/R-96-013 (NTIS PB97-115406), Office of Air Quality Planning and Standards, Research Triangle Park, NC (1996).

Barin, I., Knacke, O., and Kubaschewski, O., Thermochemical properties of inorganic substances, Springer-Verlag, New York, NY (1973).

Barin, I., Knacke, O., and Kubaschewski, O., Thermochemical properties of inorganic substances, supplement, Springer-Verlag, New York, NY (1977).

Barin, I., Thermochemical data of pure substances, VCH Verlagsgesellschaft, New York, NY (1989).

Barin, I., Thermochemical data of pure substances, VCH Verlagsgesellschaft, New York, NY (1993).

CARB Method 501- Determination of Size Distribution of Particulate Matter Emissions from Stationary Sources. State of California Air Resources Board Stationary Source Test Methods: Volume 1 - Methods for Determining Compliance with District Nonvehicular (Stationary Source) Emission Standards. Adopted March 23, 1988; amended September 12, 1990.

Chase, M.W. Jr., JANAF thermochemical tables, 3rd ed., parts 1&2, American Institute of Physics, New York, NY (1986).

Cheng, R.J., Mohnen, V.A., Shen, T.T., Current, M., and Hudson, J.B., Characterization of particulates from power plants, *J. Air Poll Control Assoc.*, 26(8), 787- 790 (1976).

Cox, J.D., Wagman, D.D., and Medvedev, V.A., CODATA Key Values for Thermodynamics, Hemisphere Publishing Corp., New York, NY (1989).

Davis, S.B, Gale, T.K., Wendt, J.O.L., and Linak, W.P., Multicomponent coagulation and condensation of toxic metals in combustors, *27th Comb. (Int.) Symp.*, 1785-1791, Comb. Inst., Pittsburgh, PA (1998).

Dockery, D.W., Pope, C.A., III, Xu, X., Spengler, J.D., Ware, J.H., Fay, M.E., Ferris, B.G., Jr., and Speizer, F.E., An association between air pollution and mortality in six U.S. cities, *New England J. Med.*, 329, 1753-1759 (1993).

Dreher, K., Costa, D., Hoffman, A., Bonner, J., and Osornio-Vargas, A., Pulmonary toxicity of urban air particulate matter (PM), Air & Waste Management Association Meeting on Measurement of Toxic and Related Air Pollutants, Research Triangle Park, NC, May 1996a.

Dreher, K., Jaskot, R., Richards, J.H., Lehmann, J.R., Winsett, D., Hoffman, A., and Costa, D., Acute pulmonary toxicity of size-fractionated ambient air particulate matter, *Amer. J. Respir. Crit. Care Med.*, 153(4:A15) (1996b).

Dreher, K., Jaskot, R., Lehmann, J.R., Richards, J.H., McGee, J.K., Ghio, A.J., and Costa, D.L., Soluble transition metals mediate residual oil fly ash induced lung injury, *J. Toxicol. Environ. Health*, 50, 285-305 (1997).

Ebbinghaus, B.B., Thermodynamics of gas phase chromium species: the chromium chlorides, oxychlorides, fluorides, oxyfluorides, hydroxides, oxyhydroxides, mixed oxyfluorochlorohydroxides, and volatility calculations in waste incineration processes, *Combust. & Flame*, 101, 119-137 (1993).

Ebbinghaus, B.B., Thermodynamics of gas phase chromium species: the chromium oxides, chromium oxyhydroxides, and volatility calculations in waste incineration processes, *Combust. & Flame*, 93, 311-338 (1995).

EPA Test Method 1A - Sample and Velocity Traverses for Stationary Sources with Small Stacks or Ducts, in 40 CFR Part 60 Appendix A, Government Institutes Inc, Rockville, MD, July 1994a.

EPA Test Method 5 - Determination of Particulate Emissions from Stationary Sources, in 40 CFR Part 60 Appendix A, Government Institutes Inc, Rockville, MD, July 1994b.

Federal Register, 62 FR 38652, July 18, 1997.

Frandsen, F., Dam-Johansen, K., and Rasmussen, P., Trace elements from combustion and gasification of coal - an equilibrium approach, *Prog. Energy Combust. Sci.*, 20, 115-138 (1994).

Galbreath, K.C., Zygarlicke, C.J., Huggins, F.E., Huffman, G.P., and Wong, J.L., Chemical speciation on nickel in residual oil ash, *Energy &Fuels*, 12, 818-822 (1998).

Garg, S., EPA Method 0060 - Methodology for the Determination of Metals Emissions in Exhaust Gases from Hazardous Waste Incineration and Similar Combustion Processes, in Methods Manual for Compliance with the BIF Regulations: Burning Hazardous Waste in Boilers and Industrial Furnaces, EPA/530-SW-91-010 (NTIS PB91-120006), pp. 3-1 through 3-48, Office of Solid Waste, Washington, DC, December 1990.

Gelbard, F., and Seinfeld, J.H., Simulation of multicomponent aerosol dynamics. *J. Colloid Interface Sci.*, 78(2), 485-501, (1980).

Goldstein H.L., and Siegmund, C.W., Influence of heavy fuel oil composition and boiler combustion conditions on particulate emissions, *Environ. Sci. & Technol.*, 10(12), 1109-1114 (1976).

Goldstein H.L., and Siegmund, C.W., Particle emissions from residual fuel fired boilers: influence of combustion modifications, *J. of Engineering Power*, 371-377 (1977).

Gurvich, L.V., Veyts, I.V., and Alcock, C.B., Thermodynamic Properties of Individual Substances, 4th ed. Vol. 2, Pts. 1&2, Hemisphere Publishing Corp., Washington, DC (1991).

Huggins, F.E., and Huffman, G.P., Speciation of elements in NIST particulate matter SRMs 1648 and 1650, *J. Hazardous Materials*, in press (1999).

Linak, W.P., and Wendt, J.O.L., "Toxic metal emissions from incineration: mechanisms and control," *Prog. Energy Combust. Sci.*, 19, 145-185 (1993).

Linak, W.P., and Wendt, J.O.L., "Trace metal transformation mechanisms during coal combustion," *Fuel Process. Technol.*, 39, 173-198 (1994).

Linak, W.P., Srivastava, R.K., and Wendt, J.O.L., Metal aerosol formation in a laboratory swirl flame incinerator," *Combust. Sci. Technol.*, 101(1-6), 7-27 (1994).

Linak, W.P., Ryan, J.V., and Wendt, J.O.L., Formation and destruction of hexavalent chromium in a laboratory swirl flame incinerator, *Combust. Sci. Technol.*, 116-117, 479-498 (1996).

Matsoukas, T., and Friedlander, S.K., Dynamics of aerosol agglomerate formation. *J. Colloid Interface. Sci.*, 146(2), 495-506, (1991).

McBride, B.J., Gordon, S., and Reno, M.A., Coefficients for calculating thermodynamic and transport properties of individual species, NASA Technical Memorandum 4513 (1993).

Miller, C.A., Linak, W.P., King, C., and Wendt, J.O.L., Fine particle emissions from heavy fuel oil combustion in a firetube package boiler, *Combust. Sci. and Technol.*, 134, 477-502, (1998).

National Research Council, "Review of EPA's Particulate Matter Research Program," National Academy Press, Washington, DC, 1998.

Owens, T., Wu, C.Y., and Biswas, P., An equilibrium analysis for reaction of metal compounds with sorbents in high temperature systems, *Chem. Eng. Comm.*, 133, 31-52 (1995).

Scotto, M.A., Peterson, T.W., and Wendt, J.O.L., Hazardous waste incineration: the *in-situ* capture of lead by sorbents in a laboratory down-flow combustor, *24th Comb. (Int.) Symp.*, 1109-1118, Comb. Inst., Pittsburgh, PA (1992).

Steele, W.J., Williamson, A.D., and McCain, J.D., Construction and operation of a 10 cfm sampling system with a 10:1 dilution ratio for measuring condensable emissions, EPA/600-8-88-069 (NTIS PB88-198551), Air and Energy Engineering Research Laboratory, Research Triangle Park, NC, April 1988.

TAPP - Thermodynamic Properties Software, V2.2, ES Microware Inc., Hamilton, OH (1995).

U.S. Department of Energy, "Fuel Oil and Kerosene Sales 1997," DOE/EIA-0535(97), Energy Information Administration, Washington, DC, August 1998.

U.S. Environmental Protection Agency, National Ambient Air Quality Standards for Particulate Matter: proposed decision, 40 CFR, Part 50 (1996a).

U.S. Environmental Protection Agency, Compilation of Air Pollutant Emission Factors Volume 2: Stationary Point and Area Sources, AP-42, 5th Ed., U.S. EPA, Office of Air Quality Planning and Standards, Research Triangle Park, NC, November 1996b.

Williams, A., Fundamentals of oil combustion, *Prog. Energy Combust. Sci.*, 2, 167-179 (1976).

Wilson, R., and Spengler, J.D., eds., Particles in Our Air: Concentrations and Health Effects, Harvard Univ. Press, Cambridge, MA (1996).

Wolff, G.T., Closure by the Clean Air Scientific Advisory Committee (CASAC) on the staff paper for particulate matter, EPA-SAB-CASAC-LTR-96-008, U.S. Environmental Protection Agency, Washington, DC, June 13, 1996.

Wu, C.Y., and Biswas, P., An equilibrium analysis to determine the speciation of metals in an incinerator, *Combust. & Flame*, 93, 31-40 (1993).

Table 1. Vanadium, nickel, zinc, iron, copper, lead, and chromium species considered for equilibrium calculations.

VANADIUM		NICKEL		ZINC		IRON		COPPER		LEAD		CHROMIUM	
Species	Reference	Species	Reference	Species	Reference	Species	Reference	Species	Reference	Species	Reference	Species	Reference
V	J6/73	Ni	J12/76	Zn	L7/93	Fe	J3/78	Cu	J9/84	Pb	J12/65	Cr	J6/79
VN	J12/73	NiO	L2/84	ZnO	L1/67	FeC_2O_4	J3/78	CuO	J12/77	PbO	J12/71	CrN	J12/73
VO	J12/73	$Ni(CO)_4$	B5/89	Zn(s)	CODA89	FeO	J9/66	Cu_2	J9/66	PbS	J6/73	$CrO(OH)_2$	BE95
VO_2	J12/73	NiO_2H_2	L3/84	Zn(l)	CODA89	$Fe(OH)_2$	J12/66	Cu(s)	CODA89	Pb_2	J9/63	$Cr(OH)_2$	BE95
V(s)	J6/73	Ni(s)	J12/76	$ZnSO_4$(a)	L3/79	FeO_2H_2	J12/66	Cu(l)	CODA89	PbH	B5/89	$Cr(OH)_3$	BE95
V(l)	J6/73	Ni(l)	J12/76	$ZnSO_4$(b)	L3/79	$Fe_2N(s)$	BAR73	CuO(s)	J12/77	Pb(s)	TPIS91	$Cr(OH)_4$	BE95
VN(s)	J12/73	NiS(a)	J12/76	ZnO(s)	BM5/84	Fe_4N(a)	BAR77	$CuO_2H_2(s)$	J6/66	Pb(l)	TPIS91	$Cr(OH)_5$	BE95
VO(s)	J12/73	NiS(b)	J12/76	$ZnO_2H_2(s)$	L7/76	Fe_4N(b)	BAR77	$CuSO_4(s)$	J6/66	PbO(rd)	J12/71	$Cr(OH)_6$	BE95
VO(l)	J12/73	NiS(l)	J12/76	ZnS(s)	BM5/84	Fe(a)	J3/78	$Cu_2O(s)$	J12/77	PbO(yw)	J12/71	$CrO(OH)_4$	BE95
$V_2O_3(s)$	J12/73	$NiS_2(s)$	J3/77	ZnS(l)	BM5/84	Fe(b)	J3/78	$Cu_2O(l)$	J12/77	PbO(l)	J12/71	CrO,OH	BE95
$V_2O_3(l)$	J12/73	$NiS_2(l)$	J3/77			Fe(c)	J3/78	$Cu_2O_2S(s)$	J6/66	$PbO_2(s)$	J12/71	$CrO(OH)_4$	BE95
V_3O_4(I)	J6/73	Ni_3S_2 (I)	J12/76			Fe(d)	J3/78	$CuCO_3(s)$	BAR77	PbS(s)	J6/73	CrO	BE95
V_3O_4(II)	J6/73	Ni_3S_2(II)	J12/76			Fe(l)	J3/78	$CuFe_2O_4$(1)	BAR77	PbS(l)	J6/73	CrO_4	BE95
$V_3O_4(l)$	J6/73	$Ni_3S_2(l)$	J12/76			$FeC_2O_4(l)$	J3/78	$CuFe_2O_4$(2)	BAR77	$Pb_3O_4(s)$	J12/71	$CrO_2(OH)_2$	BE95
$V_2O_5(s)$	J6/73	$Ni_3S_4(s)$	J3/77			FeO(s)	J6/65	$CuFe_2O_4$(3)	BAR77	$PbCO_3(s)$	B5/89	CrO_3	BE95
$V_2O_5(l)$	J6/73	$NiSO_4(s)$	IB1993			FeO(l)	J6/65	CuS(s)	BAR73	$PbSO_4$(1)	BAR73	CrOH	BE95
$VOSO_4(s)$	USBM87	$Cr_2NiO_4(s)$	IB1993			FeS(a)	J9/77	$Cu_2Fe_2O_4$(1)	BAR77	$PbSO_4$(2)	BAR73	CrOOH	BE95
		$Ni_3C(s)$	B5/89			FeS(b)	J9/77	$Cu_2Fe_2O_4$(2)	BAR77	$PbSO_4(l)$	BAR73	Cr(s)	J6/73
		$NiCO_3(s)$	B5/89			FeS(c)	J9/77	$Cu_2Fe_2O_4(l)$	BAR77			Cr(l)	J6/73
		$NiFe_2O_4$(1)	BAR73			FeS(l)	J9/77	Cu_2S(1)	BAR73			CrN(s)	J12/73
		$NiFe_2O_4$(2)	BAR73			$FeSO_4(s)$	J6/66	Cu_2S(2)	BAR73			$Cr_2N(s)$	J12/73
		NiO(1)	BAR73			$FeS_2(s)$	J9/77	Cu_2S(3)	BAR73			$Cr_2O_3(s)$	J12/73
		NiO(2)	BAR73			$Fe_2O_3(s)$	J6/65	$Cu_2S(l)$	BAR73			$Cr_2O_3(l)$	J12/73
		NiO(3)	BAR73			$Fe_2S_3O_{12}(s)$	J6/66					$Cr_3C_4(s)$	BE93
						$Fe_3O_4(s)$	J6/65					$Cr(CO)_6(s)$	BE93
						$Cr_2FeO_4(s)$	IB1993					$Cr_2(SO_4)_3(s)$	BE93
						$Fe(OH)_2(s)$	IB1993					$Cr_2FeO_4(s)$	BE93
						$Fe(OH)_3(s)$	IB1993					$Cr_2NiO_4(s)$	BE93
						$CuFe_2O_4$(1)	BAR77					$Cr_7C_3(s)$	BE93
						$CuFe_2O_4$(2)	BAR77					$Cr_3C_2(s)$	BE93
						$CuFe_2O_4$(3)	BAR77					$CrO_2(s)$	BE93
						$Cu_2Fe_2O_4$(1)	BAR77					$CrO_3(s)$	BE93
						$Cu_2Fe_2O_4$(2)	BAR77					$CrO_3(l)$	BE93
						$Cu_2Fe_2O_4(l)$	BAR77					CrS(1)	BAR77
												CrS(2)	BAR77

J9/63: JANAF 9/63 - Chase (1986)
J6/65: JANAF 9/65 - Chase (1986)
J12/65: JANAF 12/65 - Chase (1986)
J6/66: JANAF 6/66 - Chase (1986)
J9/66: JANAF 9/66 - Chase (1986)
J12/66: JANAF 12/66 - Chase (1986)
J12/71: JANAF 12/71 - Chase (1986)
J6/73: JANAF 6/73 - Chase (1986)
J12/73: JANAF 12/73 - Chase (1986)
J12/76: JANAF 12/76 - Chase (1986)
J3/77: JANAF 3/77 - Chase (1986)
J9/77: JANAF 9/77 - Chase (1986)
J12/77: JANAF 12/77 - Chase (1986)
J3/78: JANAF 3/78 - Chase (1986)
J6/79: JANAF 6/79 - Chase (1986)
J9/84: JANAF 9/84 - Chase (1986)

L1/67: Lewis 1/67 - McBride et al. (1993)
L7/76: Lewis 7/76 - McBride et al. (1993)
L3/79: Lewis 3/79 - McBride et al. (1993)
L2/84: Lewis 2/84 - McBride et al. (1993)
L3/84: Lewis 3/84 - McBride et al. (1993)
L7/93: Lewis 7/93 - McBride et al. (1993)

BAR73 - Barin (1973)
BAR77 - Barin (1977)
B5/89 - Barin (1989)
IB1993 - Barin (1993)

BE93 - Ebbinghaus (1993)
BE95 - Ebbinghaus (1995)

BM5/84: Bureau of Mines 5/84 - TAPP (1995)
USBM87: Bureau of Mines 87 - TAPP (1995)

CODA89 (Cox et al., 1989): - McBride et al. (1993)
TPIS91 (Gurvich et al., 1991): - McBride et al. (1993)

Table 2. Elemental concentrations used for equilibrium calculations.[1]

FUEL ULTIMATE ANALYSIS	g	g-moles
C	85.49	7.12
H	10.36	10.28
N	0.35	0.025
S	2.33	0.073
O	0.92	0.058
H_2O	0.50	0.028
Ash	0.10	NA[2]

FUEL TRACE ELEMENTS[3]	g	g-moles
Cr	1.05e-4	2.02e-6
Cu	3.50e-4	5.51e-6
Fe	2.10e-3	3.76e-5
Pb	4.50e-4	2.17e-6
Ni	3.00e-3	5.11e-5
V	2.20e-2	4.32e-4
Zn	7.40e-3	1.13e-4

AIR[4]	L	g-moles
O_2	260.29	11.62
N_2	979.55	43.73

[1]Basis: 100 g of oil.
[2]Not applicable.
[3]Trace elements > 1 μg/g of oil.
[4]20% excess air.

Table 3. Comparison of calculated mass concentrations determined from measured volume PSDs with measured mass concentrations determined by EPA M-5.

	VOLUME CONCENTRATIONS (MEASURED) ($\mu m^3/cm^3$)		MASS CONCENTRATIONS (CALCULATED) (mg/m^3)[1]		MASS CONCENTRATIONS (MEASURED) (mg/m^3)[2]	
	BOILER	COMBUSTOR	BOILER	COMBUSTOR	BOILER	COMBUSTOR
SMPS	8.8e+1	2.7e+4	3.1e-1	9.3e+1	-	-
INSITEC	9.8e+4	1.9e+2	1.8e+2	3.6e-1	-	-
TOTAL	9.8e+4	2.7e+4	1.8e+2	9.3e+1	184 (6.2)[3]	93

[1]Assumed fine mode particle density = 3.5 g/cm^3 based on typical densities for vanadium species. Assumed coarse mode particle density = 1.85 g/cm^3.
[2]Measured mass concentrations determined using EPA Method 5.
[3]Number in parentheses indicated standard deviation based on multiple measurements.

Table 4. Comparison of trace element emissions for high sulfur No. 6 oil from two combustion systems ($\mu g/m^3$).

ELEMENT	BOILER	COMBUSTOR
Sb	7.7	-
As	6.3	-
Be	0.09	-
Cd	3.5	-
Cr	11.	-
Cu	170.	200.
Fe	740.	1200.
Pb	89.	-
Mg	1200.	1700.
Mn	16.	-
Hg	< 2.2	-
Ni	1200.	1400.
Na	-	2100.
V	9800.	12000.
Zn	3300.	3000.

LIST OF FIGURES

Fig. 1 1997 U.S. residual fuel oil sales by location and end use. Total sales equal 47.3×10^9 L (12.5×10^9 gal). The 13 other Great Plains and Rocky Mountain States combined account for less than 1% of total sales (adapted from U.S. DOE, 1998).

Fig. 2 Two EPA combustion systems.

Fig. 3 EPA dilution sampling system.

Fig. 4 Fuel oil droplet PSDs from the fire-tube boiler atomizer.

Fig. 5 Residual fuel oil equilibrium predictions.

Fig. 6 Measured volume and calculated mass PSDs.

Fig. 7 SEM image of fuel oil char from the fire-tube boiler.

Fig. 8 Elemental PSDs determined from impactor samples from the refractory-lined combustor.

Fig. 9 Predicted evolution of PSDs via coagulation.

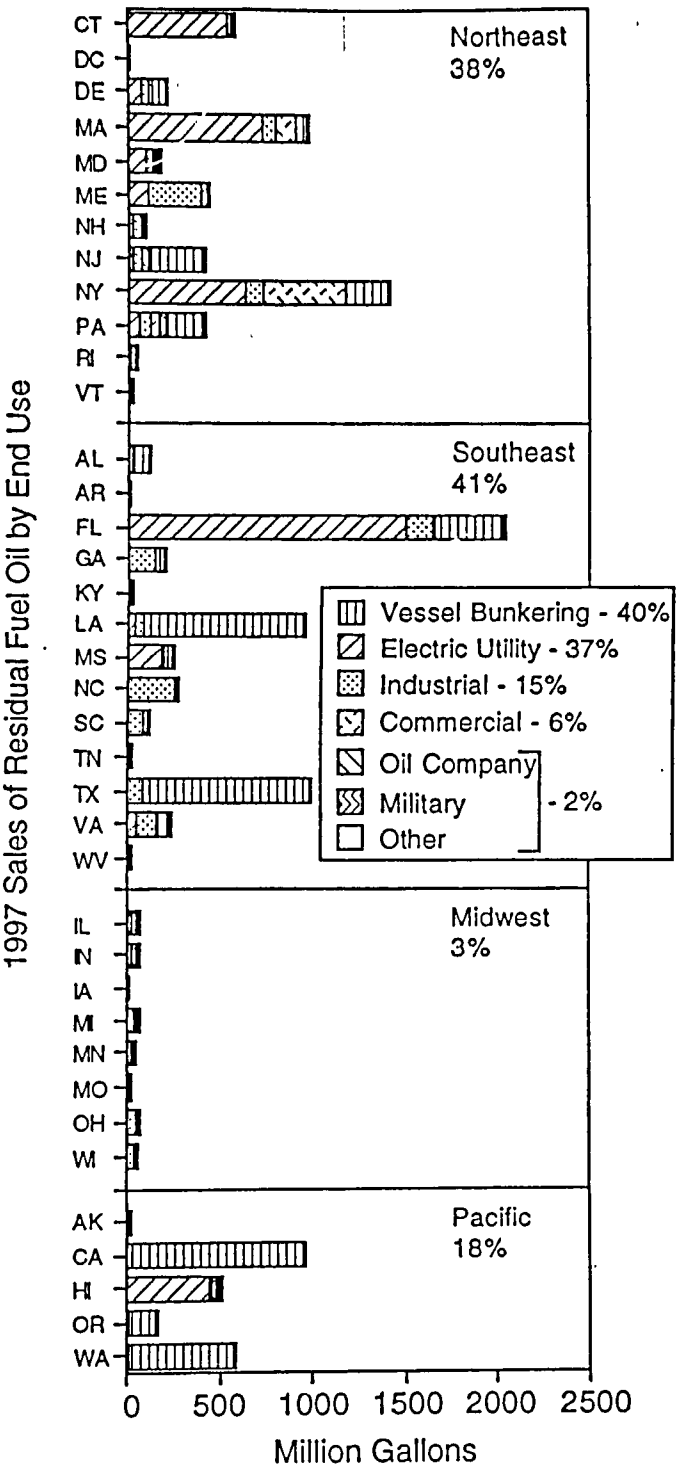
1997 Sales of Residual Fuel Oil by End Use
CT
DC
DE
MA
MD
ME
NH
NJ
NY
PA
RI
VT
AL
AR
FL
GA
KY
LA
MS
NC
SC
TN
TX
VA
WV
IL
IN
IA
MI
MN
MO
OH
WI
AK
CA
HI
OR
WA
Northeast
38%
Southeast
41%
Midwest
3%
Pacific
18%
Vessel Bunkering - 40%
Electric Utility - 37%
Industrial - 15%
Commercial - 6%
Oil Company
Military
Other
- 2%
0
500
1000
1500
2000
2500
Million Gallons

Figure 1

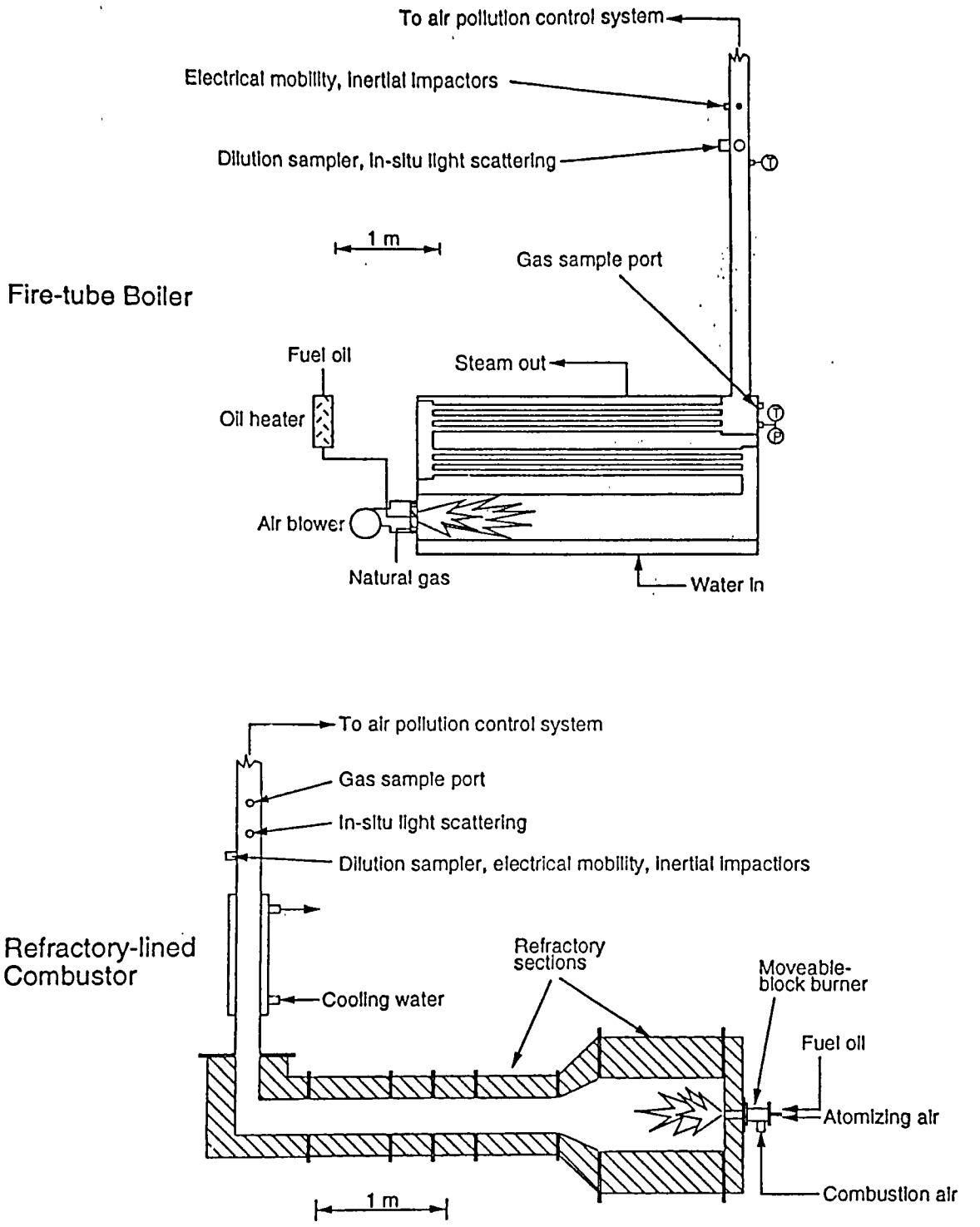
To air pollution control system
Electrical mobility, inertial impactors
Dilution sampler, in-situ light scattering
1 m
Gas sample port
Fire-tube Boiler
Fuel oil
Steam out
Oil heater
Air blower
Natural gas
Water in
To air pollution control system
Gas sample port
In-situ light scattering
Dilution sampler, electrical mobility, inertial impactiors
Refractory-lined Combustor
Refractory sections
Moveable-block burner
Cooling water
Fuel oil
Atomizing air
Combustion air
1 m

Figure 2

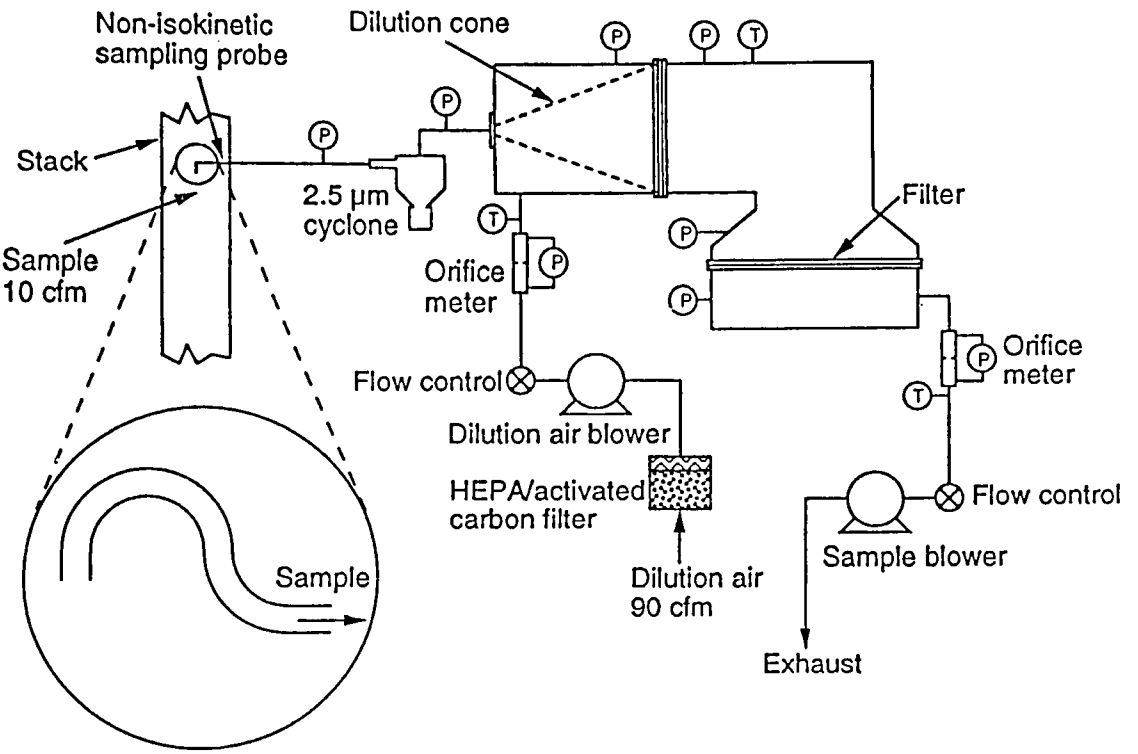
Non-isokinetic
sampling probe
Dilution cone
Stack
Sample
10 cfm
2.5 µm
cyclone
Orifice
meter
Filter
Orifice
meter
Flow control
Dilution air blower
HEPA/activated
carbon filter
Flow control
Sample blower
Dilution air
90 cfm
Exhaust
Sample

Figure 3

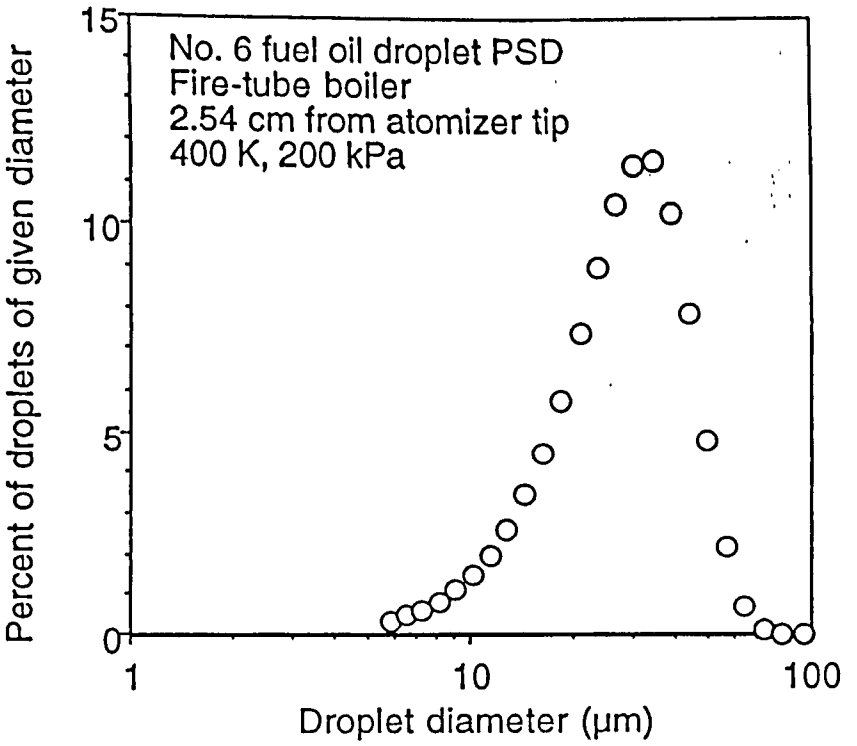
No. 6 fuel oil droplet PSD
Fire-tube boiler
2.54 cm from atomizer tip
400 K, 200 kPa
Percent of droplets of given diameter
15
10
5
0
1
10
100
Droplet diameter (μm)

Figure 4

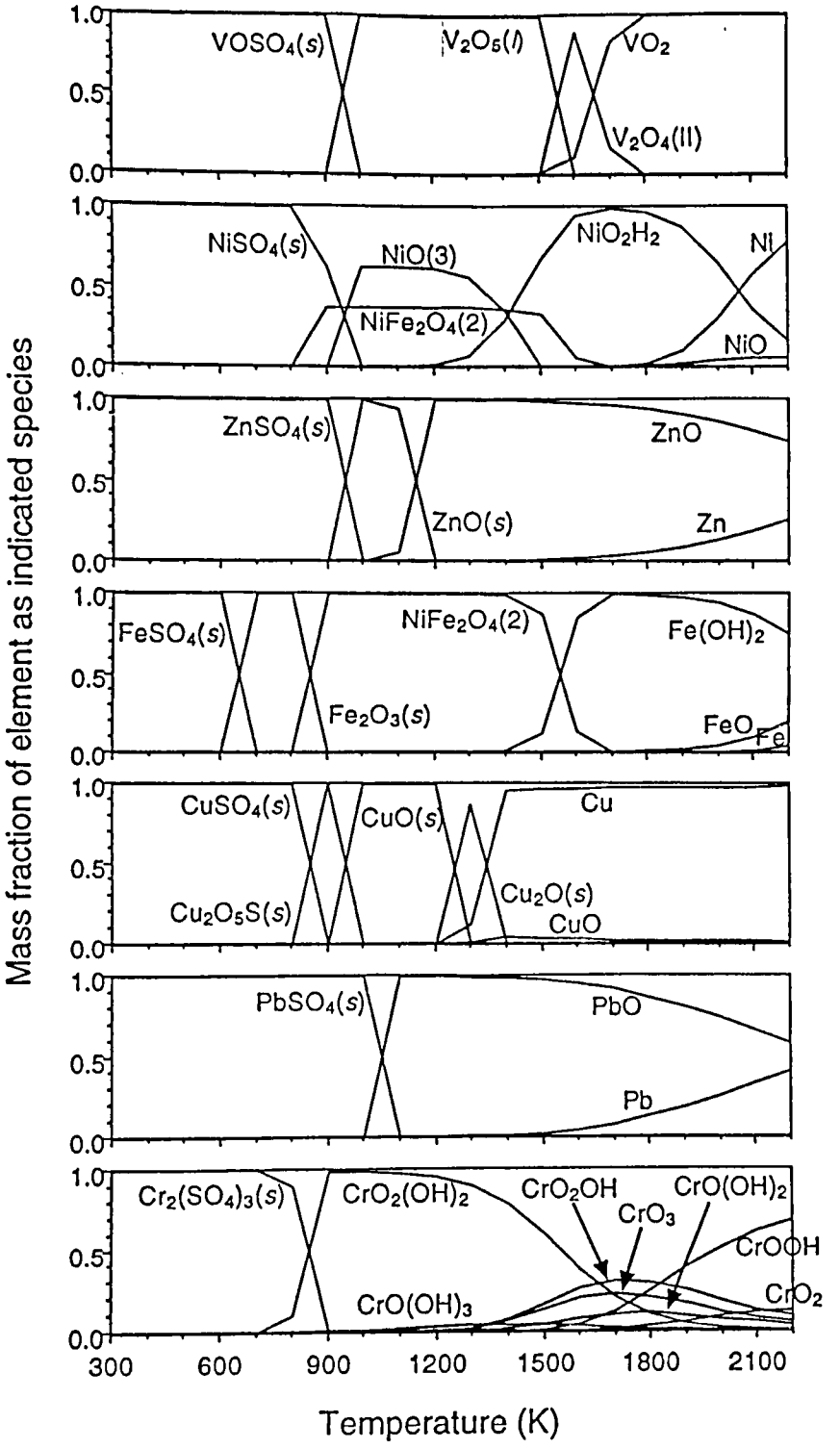
Mass fraction of element as indicated species
1.0
0.5
0.0
VOSO4(s)
V2O5(l)
VO2
V2O4(II)
NiSO4(s)
NiO(3)
NiO2H2
Ni
NiFe2O4(2)
NiO
ZnSO4(s)
ZnO
ZnO(s)
Zn
FeSO4(s)
NiFe2O4(2)
Fe(OH)2
Fe2O3(s)
FeO
Fe
CuSO4(s)
CuO(s)
Cu
Cu2O5S(s)
Cu2O(s)
CuO
PbSO4(s)
PbO
Pb
Cr2(SO4)3(s)
CrO2(OH)2
CrO2OH
CrO3
CrO(OH)2
CrOOH
CrO(OH)3
CrO2
300
600
900
1200
1500
1800
2100
Temperature (K)

Figure 5

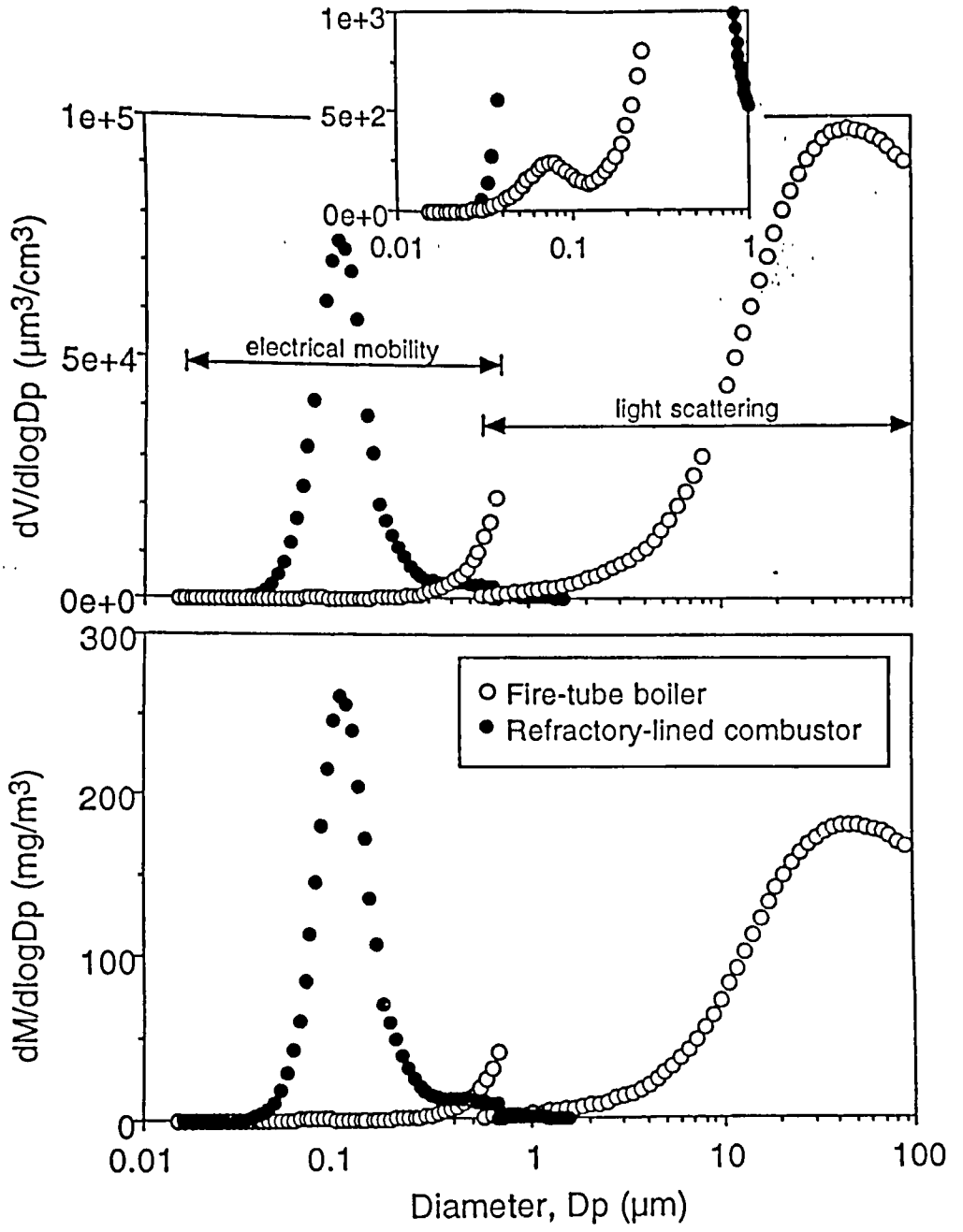
1e+3
5e+2
0e+0
0.01
0.1
1
1e+5
5e+4
0e+0
dV/dlogDp (µm3/cm3)
electrical mobility
light scattering
300
200
100
0
dM/dlogDp (mg/m3)
Fire-tube boiler
Refractory-lined combustor
0.01
0.1
1
10
100
Diameter, Dp (µm)

Figure 6

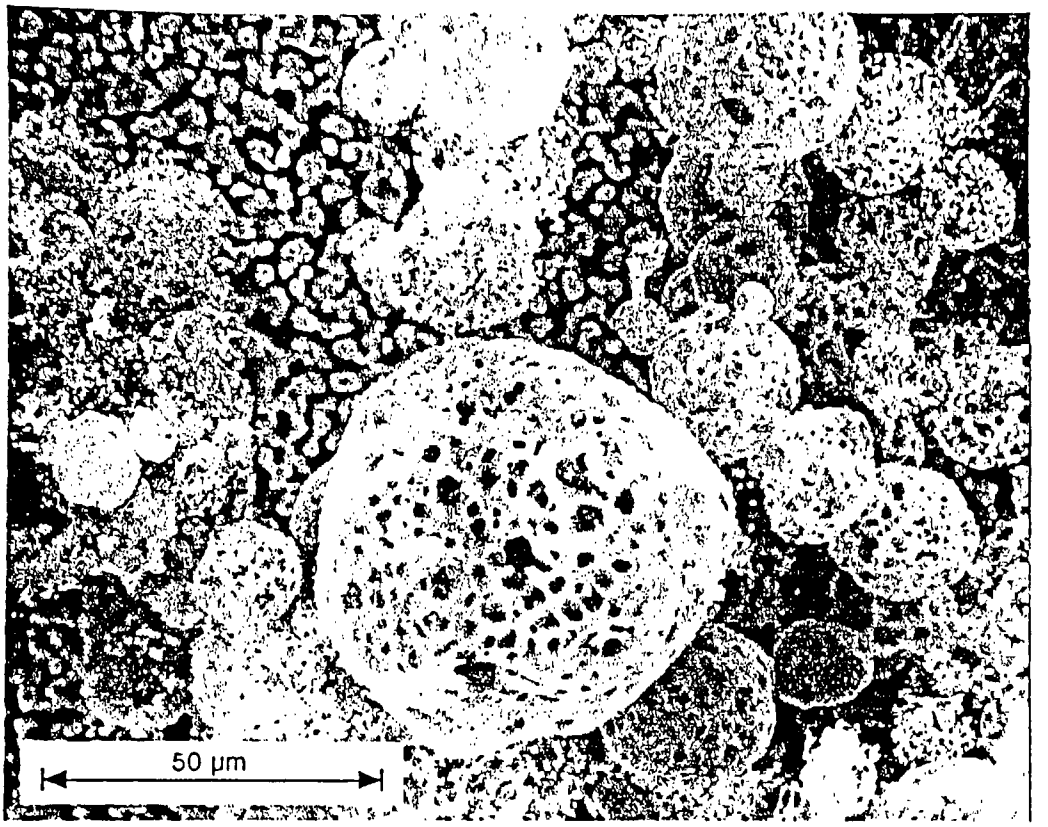

Figure 7

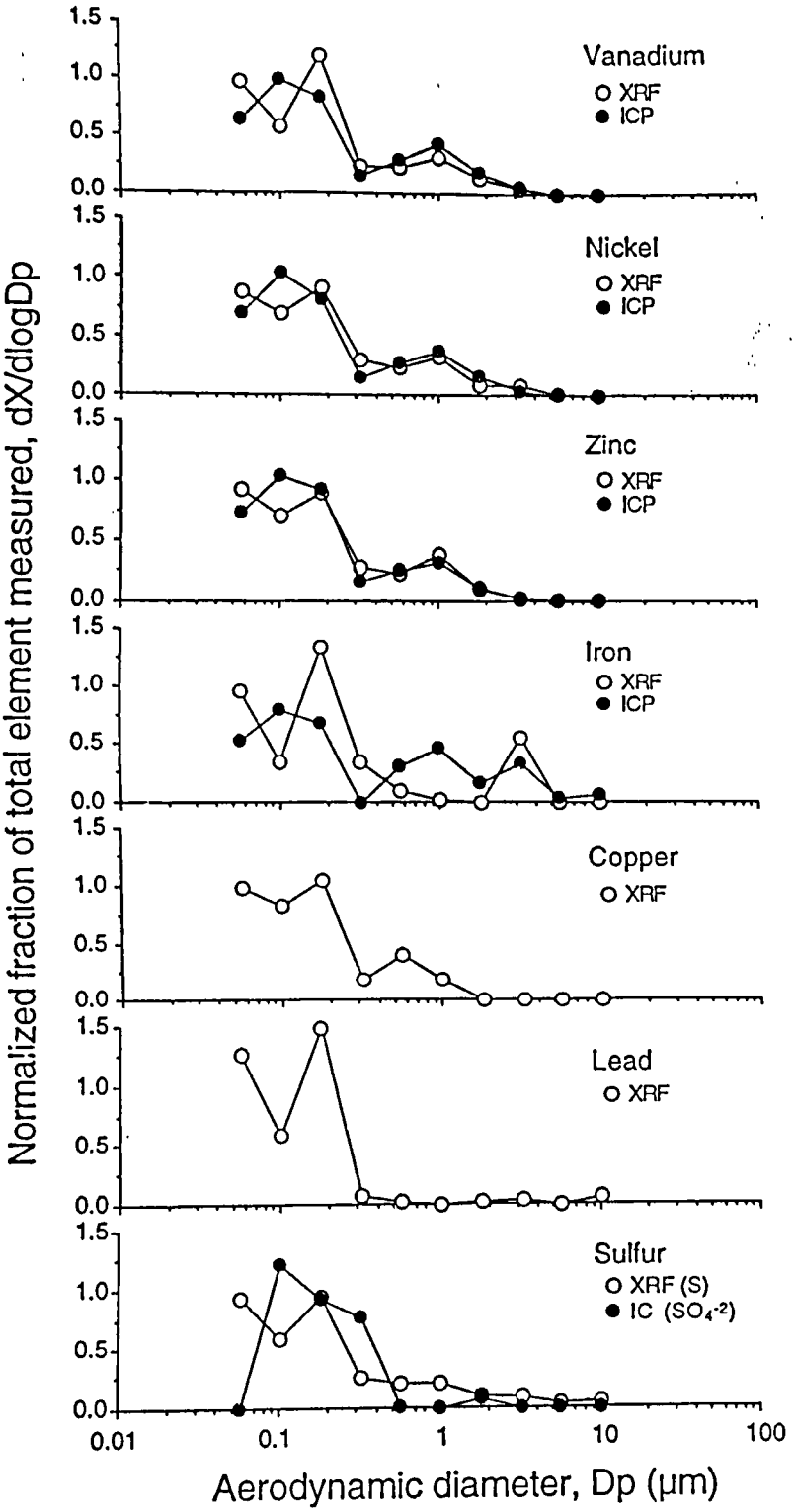
Normalized fraction of total element measured, dX/dlogDp
Vanadium
O XRF
● ICP
Nickel
O XRF
● ICP
Zinc
O XRF
● ICP
Iron
O XRF
● ICP
Copper
O XRF
Lead
O XRF
Sulfur
O XRF (S)
● IC (SO_4^{-2})
1.5
1.0
0.5
0.0
0.01
0.1
1
10
100
Aerodynamic diameter, Dp (μm)

Figure 8

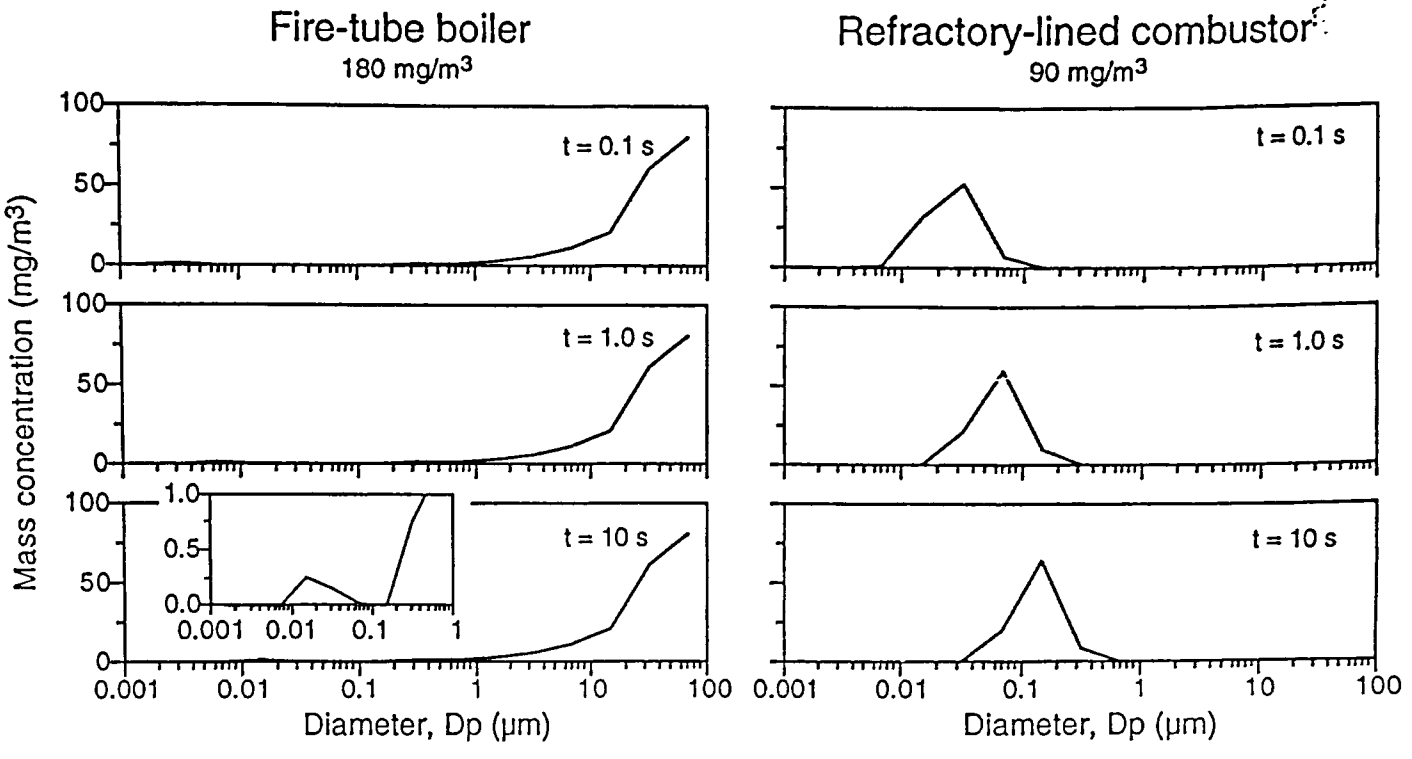
Fire-tube boiler
180 mg/m3
Refractory-lined combustor
90 mg/m3
Mass concentration (mg/m3)
t = 0.1 s
t = 1.0 s
t = 10 s
100
50
0
1.0
0.5
0.0
0.001
0.01
0.1
1
10
100
Diameter, Dp (μm)

Figure 9